J|A|C|S ARTICLES

Published on Web 06/03/2010

Intramolecular Electronic Interactions between Nonconjugated Arene and Quinone Chromophores

Georg Jansen,* Björn Kahlert, Frank-Gerrit Klärner,* Roland Boese, and Dieter Bläser

Institut für Organische Chemie and Institut für Anorganische Chemie, Universität Duisburg-Essen, 45117 Essen, Germany

Received December 14, 2009; E-mail: georg.jansen@uni-duisburg-essen.de; frank.klaerner@uni-duisburg-essen.de

Abstract: The novel surprisingly colorful dark blue and orange-red molecular clips **1** and **2** containing a central *p*-benzoquinone spacer-unit and anthracene or napththalene sidewalls were synthesized by DDQ oxidation of the corresponding colorless hydroquinone clips **7** and **8**. The colors of the quinone clips result from broad absorption bands in the visible range (**1**, $\lambda_{max} = 537$ nm and **2**, $\lambda_{max} = 423$ and $\lambda_{shoulder} = 515$ nm) showing bathochromic shifts of 112 and 90 nm, respectively, compared to the similarly tetraalkyl-substituted duroquinone **31**, even though the clips **1** and **2** only contain insulated π systems as chromophores, a central tetraalkyl-substituted *p*-benzoquinone spacer-unit and two anthracene or two naphthalene sidewalls. To elucidate the electronic properties of these clips, we prepared the compound **3**, the anti-configured isomer of clip **2**, and the benzene-, naphthalene-, and anthracene-substituted quinones **4**, **5**, and **6**, the so-called "half-clips". The "half-clips" **6** and **5** show a similar color change and the same trend in the UV/vis absorption spectra as the anthracene and naphthalene clip **1** and **2**. This finding already rules out that the color of these systems is a result of "through-space" $\pi-\pi$ interactions between the aromatic sidewalls in the molecular clips **1** and **2**. Quantum chemical *ab initio* calculations provide good evidence that the bathochromic shift of the absorption band at the longest wavelength observed in the UV/vis spectra of the clip quinones **2**, **3**, and **1** and the "half-clip" quinones **4**, **5**, and **6** with an increasing number of rings in the anellated aromatic unit (from benzene to anthracene) is the result of an increasing configuration interaction between a $n \rightarrow \pi^*$ excitation of the quinoid component and a $\pi \rightarrow \pi^*$ excitation with intramolecular charge transfer (CT) character. The initial π orbitals involved here and in higher lying transitions mainly stem from through-space interactions between π orbitals of the aromatic sidewalls and π orbitals of the quinone moiety with varying degree of mixing. The configuration interaction in the excited states can be considered to be a homoconjugation, that is, the relevant charge transfer states are formed across an allegedly insulating aliphatic bridge. The UV/vis spectra of the molecular clips **1**−**3**, the "half-clips" **4**−**6**, and the quinones **32** and **33** simulated by means of quantum chemical *ab initio* calculations agree well with the experimental spectra.

Introduction

In organic molecules such as polycyclic aromatic−aliphatic systems and biomolecules like proteins and DNA, through-space and through-bond interactions have been proposed to understand the electronic interactions between π systems that are insulated by one or more saturated carbon atoms from each other.[1] These interactions are important for the understanding of spectroscopic properties (e.g., photoelectron, UV/vis absorption, and emission spectra), reactivity (for example, redox reactions), and electric conductivity of these systems.[2] For several decades, it is known that rapid long-range electron and hole transfer processes through saturated carbon bridges in donor-bridge-acceptor systems can take place with high efficiencies even for long bridges, highlighting the role of through-bond interactions.[3] A recent, surprising finding is that bridges containing π systems which are not conjugated with the donor and acceptor moieties

(1) "Through-space", "through-bond" interactions: (a) Hoffmann, R.; Heilbronner, E.; Gleiter, R. *J. Am. Chem. Soc.* **1970**, *92*, 706–707. (b) Hoffmann, R. *Acc. Chem. Res.* **1971**, *4*, 1–9. (c) Filipescu, N.; Minn, F. L.; Thomas, A. V. *J. Chem. Soc., Perkin Trans. 2* **1972**, 1697–1702. (d) Haselbach, E.; Neuhaus, L.; Johnson, R. P.; Houk, K. N.; Paddon-Row, M. N. *Helv. Chim. Acta* **1982**, *65*, 1743–1751. (e) Jordan, K. D.; Paddon-Row, M. N. *Chem. Rev.* **1992**, *92*, 395–410. Electron transfer through DNA and peptides: (f) Giese, B. *Bioorg. Med. Chem.* **2006**, *4*, 6139–6143. (g) Breeger, S.; von Meltzer, M.; Hennecke, U.; Carell, T. *Chem.−Eur. J.* **2006**, *12*, 6469–6477. (h) Boussicault, F.; Robert, M. *Chem. Rev.* **2008**, *108*, 2622–2645. (i) Elias, B.; Genereux, J. C.; Barton, J. K. *Angew. Chem., Int. Ed.* **2008**, *47*, 9067–9070. (j) Ghosh, A.; Joy, A.; Schuster, G. B.; Douki, T.; Cadet, J. *Org. Biomol. Chem.* **2008**, *6*, 916–928.

(2) (a) Caraballo-Martinez, N.; del Rosario Colorado Heras, M.; Blazquez, M. M.; Barcina, J. O.; Martinez, A. G.; del Rosario Torres Salvador, M. *Org. Lett.* **2007**, *9*, 2943–2946. (b) Bell, T. D. M.; Stefan, A.; Lemaur, V.; Bernhardt, S.; Muellen, K.; Cornil, J.; Beljonne, D.; Hofkens, J.; Van der Auweraer, M.; De Schryver, F. C. *Photochem. Photobiol. Sci.* **2007**, *6*, 406–415. (c) Kobayashi, T.; Kobayashi, S. *Eur. J. Org. Chem.* **2002**, 2066–2073.

(3) (a) Zimmerman, H. E.; McKelvey, R. D. *J. Am. Chem. Soc.* **1971**, *93*, 3638–3645. (b) Oevering, H.; Paddon-Row, M. N.; Heppener, M.; Oliver, A. M.; Cotsaris, E.; Verhoeven, J. W.; Hush, N. S. *J. Am. Chem. Soc.* **1987**, *109*, 3258–3269. (c) Paddon-Row, M. N. *Acc. Chem. Res.* **1994**, *27*, 18–25.

do not lead to increased photoinduced charge transfer rates compared to geometrically similar fully saturated bridges.[4] The charge transport through the σ system was even observed to be insensitive to changes in hybridization of the bridge carbon atoms. Hyperconjugation between neighboring π and σ systems recently was found to be nearly half as strong as conjugation between adjacent π systems.[5] π,σ hyperconjugations are also known to contribute to the interactions between the two dimethylene-bridged double bonds of norbonadiene, which are mainly attributed to direct through-space homoconjugation.[6] They were also proposed to explain the strong donor−acceptor coupling in an intramolecular triptycene quinhydrone system.[7]

Here, we report the synthesis and spectroscopic properties of the dimethylene-bridged molecular clips **1** and **2.** Even though each system only contains insulated π systems (a central *p*-benzoquinone spacer-unit and two aromatic sidewalls) and, therefore, is expected to be yellow resulting from the quinone moiety as chromophore,[8] the anthracene clip **1** is dark blue and the naphthalene clip **2** is orange-red. To elucidate the origin of the surprising color especially of clip **1**, we synthesized compound **3**, the anti-configured isomer of **2**, and the benzene-, naphthalene-, and anthracene-substituted quinones **4**− **6** and calculated the electronic spectra of **1**− **6** by ab initio methods. The anti configuration of the two arene moieties in **3**[9] and the lack the of the second arene sidewall in **4**− **6** prevent a through-space interaction between the arene moieties of the sidewalls which may be possible in the molecular clips **1** and **2**.

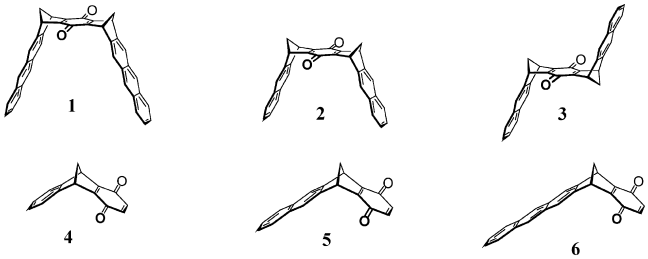

Results and Discussion

The quinone clips **1** and **2** (Figure 1) were synthesized by oxidation of the known hydroquinones **7**[10] and **8**[11] with 2,3-dichloro-5,6-dicyano-1,4-benzoquinone (DDQ). Compound **3** (Figure 2), the anti-configured isomer of **2**, was prepared

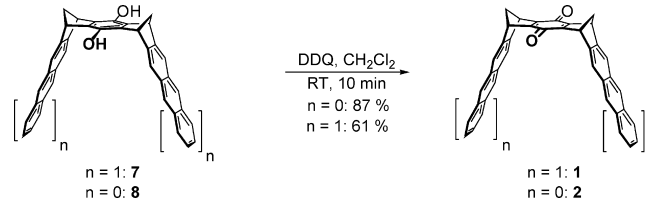

Figure 1. Synthesis of the quinone clips **1** and **2**.

analogously to **1** and **2** starting in this case by the hydrolysis of the known diacetoxy-substituted compound **9**[11] and subsequent DDQ oxidation of the hydroquinone **10** resulting from the hydrolysis.

For the synthesis of the compounds **4**−**6** (Figures 3−5), new routes were developed. Diels−Alder cycloaddition of 1,4-dichloro-1,3-butadiene **11**[12] to dimethoxybenzonorbornadiene **12**[13] followed by HCl elimination with potassium *tertiary*-butoxide without isolation of the primary Diels−Alder adduct leads in one step to the dibenzonorbornadiene derivative **13**. The methoxy groups in **13** were cleaved by BBr_3 and the resulting hydroquinone was again oxidized with DDQ producing the desired benzo-substituted quinone **4**. The synthesis of the naphthalene- and anthracene-substituted quinones **5** and **6** started both from diacetoxybenzonorbornadiene **19**[13,14] using the methodology for the anellation of naphthalene units to CC double bonds developed by Cava et al.[15] and later refined by Paddon-Row et al.[16] 1,4 Br_2-elimination of tetrabromo- or hexabromo-*o*-xylene **15** or **16** with sodium iodide led to the *o*-quinodimethane **17** or **18** as reactive intermediate which was trapped by Diels−Alder reaction with **19**. The primary Diels−Alder adduct was not stable under the conditions of reaction and eliminated two molecules of HBr leading to the benzonaphthonorbornadiene **22** and **23**, respectively. The acetoxy functions in **22** were hydrolyzed and the resulting hydroquinone **24** was again oxidized by DDQ producing the desired naphthalene-substituted quinone **5**.

For the preparation of the anthracene-substituted quinone **6**, it was necessary to convert the diacetoxybenzo-dibromonaphthalene-substituted compound **23** to the corresponding dimethoxy derivative **25**. This conversion was performed in one step by basic hydrolysis of the acetoxy groups and subsequent methylation of the resulting phenolate groups with methyl iodide. Br_2 elimination in **25** with *n*-butyllithium led to the corresponding aryne as reactive intermediate which was trapped with furan leading to a mixture of *syn*-**26** and *anti*-**26** in a ratio of (2:3) which was isolated but not separated. Deoxygenation of the mixture of *syn*-**26** and *anti*-**26** with titanium tetrachloride and zinc powder gave the anthracene-substituted dimethoxybenzonorbornadiene **27**. The methoxy groups in **27** were again cleaved with BBr_3 and the resulting hydroquinone **28** was oxidized with DDQ to give the desired anthracene-substituted quinone **6**. If a larger excess of BBr_3 (40 instead of 20 molequivalents, containing a small amount of Br_2) was used for the reaction with **27**, the 9,10-dibromoanthracene derivative **29** was isolated after DDQ oxidation of the primary product.

(4) Goldsmith, R. H.; Vura-Weis, J.; Scott, A. M.; Borkar, S.; Sen, A.; Ratner, M. A.; Wasielewski, M. R. *J. Am. Chem. Soc.* **2008**, *130*, 7659–7669.
(5) (a) Cappel, D.; Tüllmann, S.; Krapp, A.; Frenking, G. *Angew. Chem., Int. Ed.* **2005**, *44*, 3617–3620. (b) Fernandez, I.; Frenking, G. *Chem.—Eur. J.* **2006**, *12*, 3617–3629.
(6) (a) Heilbronner, E.; Schmelzer, A. *Helv. Chim. Acta* **1975**, *58*, 936–967. (b) Martin, H.-D.; Mayer, B. *Angew. Chem., Int. Ed.* **1983**, *22*, 283–314. (c) Houk, K. N.; Rondan, N. G.; Paddon-Row, M. N.; Jefford, C. W.; Thanh Huy, P.; Burrow, P. D.; Jordan, K. D. *J. Am. Chem. Soc.* **1983**, *105*, 5563–5568.
(7) Iwamura, H.; Makino, K. *J. Chem. Soc., Chem. Commun.* **1978**, 720–721.
(8) (a) Vischer, E. B. *J. Chem. Soc.* **1953**, 815–820. (b) Flaig, W.; Salfeld, J.-C. *Justus Liebigs Ann. Chem.* **1958**, *618*, 117–139.
(9) Attemps to synthesize the anti-configured anthracene clip for a comparison with clip **1** failed presumably because of the low solubility of the tetrabromoderivative of **9** which did not react with *n*-butyllithium and furan. Kahlert, B. Dissertation, University of Duisburg-Essen, 2005.
(10) Klärner, F.-G.; Kahlert, B.; Boese, R.; Blaeser, D.; Juris, A.; Marchioni, F. *Chem.—Eur. J.* **2005**, *11*, 3363–3374.
(11) Klärner, F.-G.; Panitzky, J.; Bläser, D.; Boese, R. *Tetrahedron* **2001**, 3673–3687.
(12) Bartlett, P. D.; Wallbillich, G. E. H. *J. Am. Chem. Soc.* **1969**, *91*, 409–414.
(13) Meinwald, J.; Wiley, G. A. *J. Am. Chem. Soc.* **1958**, *80*, 3667–3671.
(14) Vaughan, W. R.; Yoshimine, M. *J. Org. Chem.* **1957**, *22*, 7–12.
(15) (a) Cava, M. P.; Napier, D. R. *J. Am. Chem. Soc.* **1957**, *79*, 1701–1709. (b) Cava, M. P.; Shirley, R. L. *J. Am. Chem. Soc.* **1960**, *82*, 654–656.
(16) Paddon-Row, M. N.; Patney, H. K.; Harish, K. *Synthesis* **1986**, 328–330.

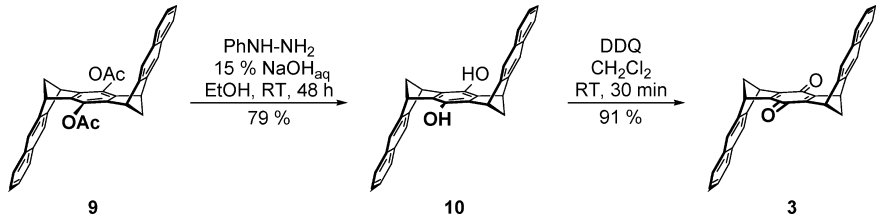

Figure 2. Synthesis of the quinone **3**.

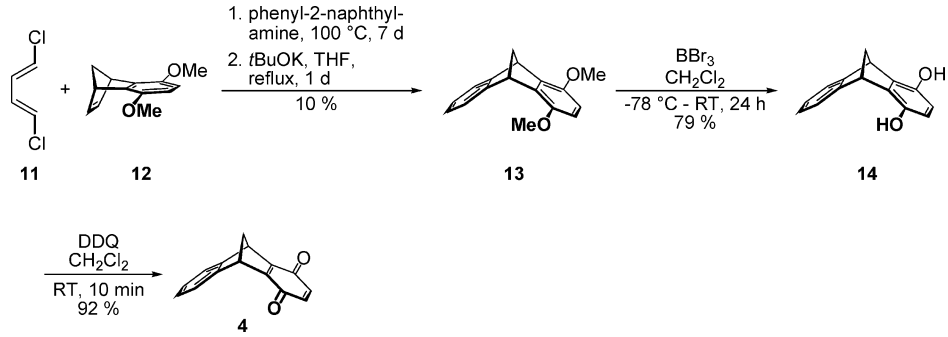

Figure 3. Synthesis of the quinone **4**.

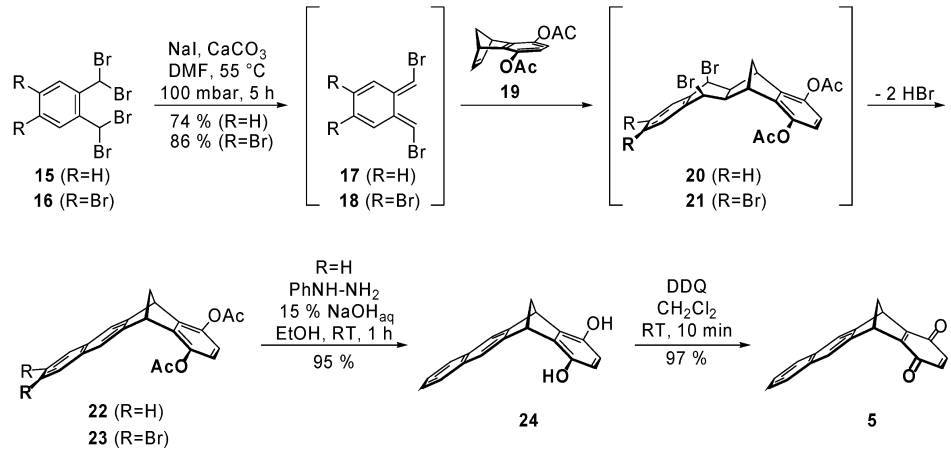

Figure 4. Synthesis of the quinone **5**.

The structures of all new compounds were assigned by the spectral data as described in the Experimental Details in Supporting Information. In the case of compounds **22**, **23**, and **27**, the precursors of the naphthalene- and anthracene-substituted quinones **5** and **6**, an independent structural proof came from single-crystal structure analysis (Figure 6). In all three systems, the naphthalene or anthracene CC bond fused to the norbornadiene moiety is remarkably longer than the other naphthalene or anthracene bonds C15−C18 d [Å] = 1.440(4), C15−C18 1.425(5), C17−C22 1.442(2) for **22**, **23** and **27**, respectively. The bond lengths in the diacetoxy- or dimethoxy-substituted benzene ring in **22**, **23**, or **27** are analogously but less strongly influenced by the fused norbornadiene unit. These findings indicate that the norbornadiene unit causes a partial localization of the π bonds in the fused arene moieties comparable to that observed in tris(bicyclo[2.1.1]hexeno)benzene[17] and tris-(bicyclo[2.2.1]hepteno)benzene derivatives.[18]

As already pointed out in the introduction, the anthracene and naphthalene quinone clips **1** and **2** are colorful substances. Crystals of **1** are dark blue almost black and those of **2** and the *anti*-isomer **3** are orange-red or orange (Figure 7). Each of the UV/vis spectra of **1**, **2**, and **3** exhibits a broad absorption band in the visible region in addition to the α, β, and p bands which are characteristic for the aromatic anthracene or naphthalene system. The absorption band of **1** at the longest wavelength (λ_{max} = 537 nm, log ε = 317) shows a bathochromic shift compared to that of **2** (λ_{max} = 423 nm, 515 nm (shoulder), log ε = 2.98, 2.58) and **3** (λ_{max} = 425 nm, log ε = 3.19). The UV/vis spectra of the isomeric naphthalene quinone **2** and **3** are very similar to each other with exception of the shoulder at λ = 515 nm only observed in the spectra of **2** (Figure 8).

The position and high intensity of these absorption bands are unusual for nonconjugated *p*-benzoquinone derivatives. For example, *p*-benzoquinone (**30**) itself and duroquinone **31** as well as the norbornadiene-anellated quinones **32** and **33** are yellow

(17) (a) Bürgi, H.-B.; Baldridge, K. K.; Hardcastle, K.; Frank, N. L.; Gantzel, P.; Siegel, J. S.; Ziller, J. *Angew. Chem., Int. Ed. Engl.* **1995**, *34*, 1454–1456. (b) Frank, N. L.; Baldridge, K. K.; Siegel, J. S. *J. Am. Chem. Soc.* **1995**, *117*, 2102–2103.

(18) (a) Frank, N. L.; Baldridge, K. K.; Gantzel, P.; Siegel, J. S. *Tetrahedron Lett.* **1995**, *36*, 4389–4392. (b) Rathore, R.; Lindemann, S. V.; Kumar, A. S.; Kochi, J. K. *J. Am. Chem. Soc.* **1998**, *120*, 6012–6018. (c) Cardullo, F.; Giuffrida, D.; Kohnke, F. H.; Raymo, F. M.; Stoddart, J. F.; Williams, D. J. *Angew. Chem., Int. Ed. Engl.* **1996**, *35*, 339–341.

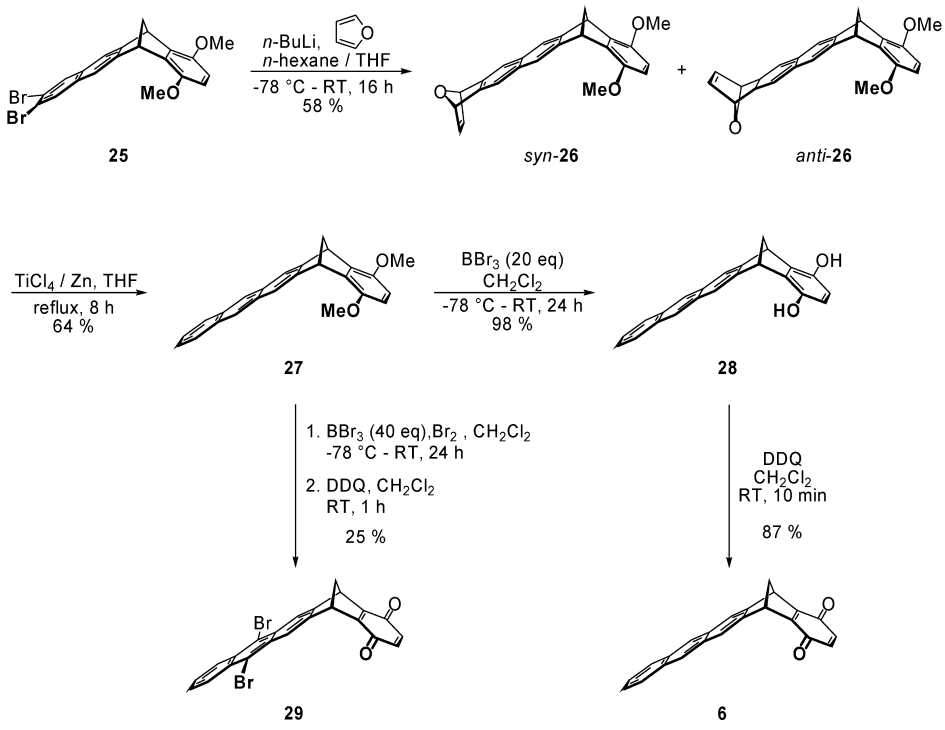

Figure 5. Synthesis of the quinones **6** and **29**.

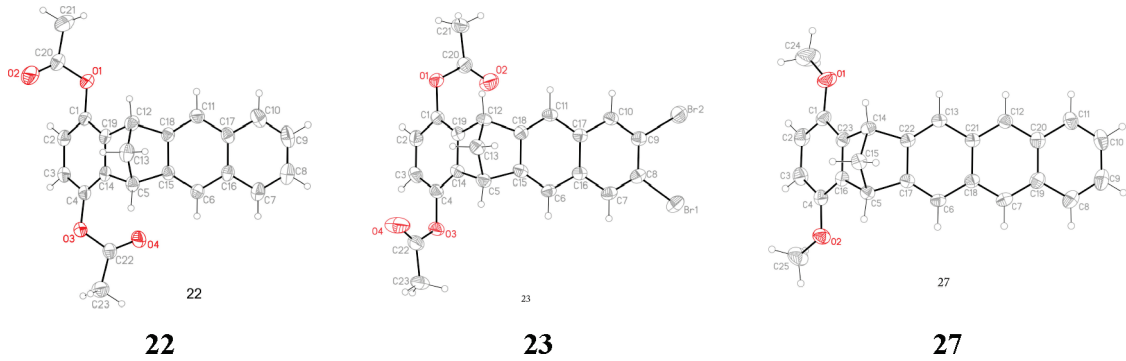

Figure 6. Single-crystal structures of the quinone precursors **22**, **23**, and **26**.

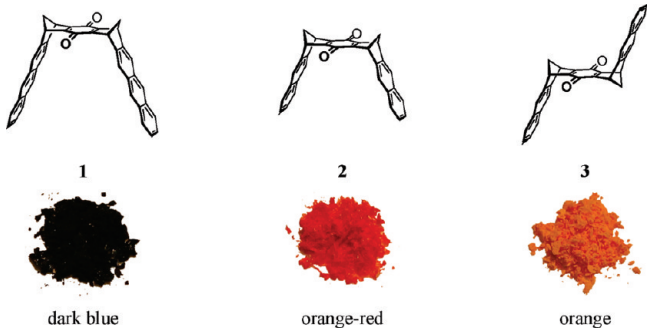

Figure 7. Structures and colors of the solids of the quinones **1**−**3**.

to orange (Figure 9)[8] showing only weak absorption bands in the visible region, however, at shorter wavelengths than the quinone clips **1** and **2**, which were assigned to the forbidden $n \rightarrow \pi^*$ transitions (Figures 10, 11).

The color of arene-substituted norbornadieno-quinones **4**, **5**, **6**, and **29** changes from yellow over blue-gray to dark violet comparable to the color change observed for naphthalene- and anthracene-substituted clips (Figures 7 and 12). The absorption band at the longest wavelength in the UV/vis spectra of the quinones **4**, **5**, and **6** shows a bathochromic shift with the transition of the benzene-substituted norbornadienoquinone **4** to the naphthalene- and finally anthracene-substituted system **5** and **6**, respectively (Figure 13). Bromosubstitution of the anthracene moiety in **29** leads to a hypsochromic shift compared to **6** (Figure 14).

The finding that the monosubstituted quinones **6** and **5** show a similar color change and the same trend in the UV/vis spectrum as the corresponding naphthalene and anthracene clip **2** and **1**, respectively, already rules out that the color of these systems is a result of a through-space $\pi-\pi$ interaction between the aromatic sidewalls in the molecular clips. To elucidate the mechanism of the bathochromic shift observed here, the UV/vis spectra of benzene (**34**); naphthalene (**35**); anthracene (**36**); *p*-benzoquinone (**30**); and the benzene-, naphthalene-, and anthracene- substituted quinones **4**, **5**, and **6**; the clips **1**, **2**, and **38** as well as the *anti*-isomers **3** and **37**, **39**, and **40** (Figure 15 were calculated by the use of quantum chemical methods, that is, by coupled-cluster theory in the CC2 approximation.[19] The underlying Hartree−Fock (HF) molecular orbitals (MOs) were

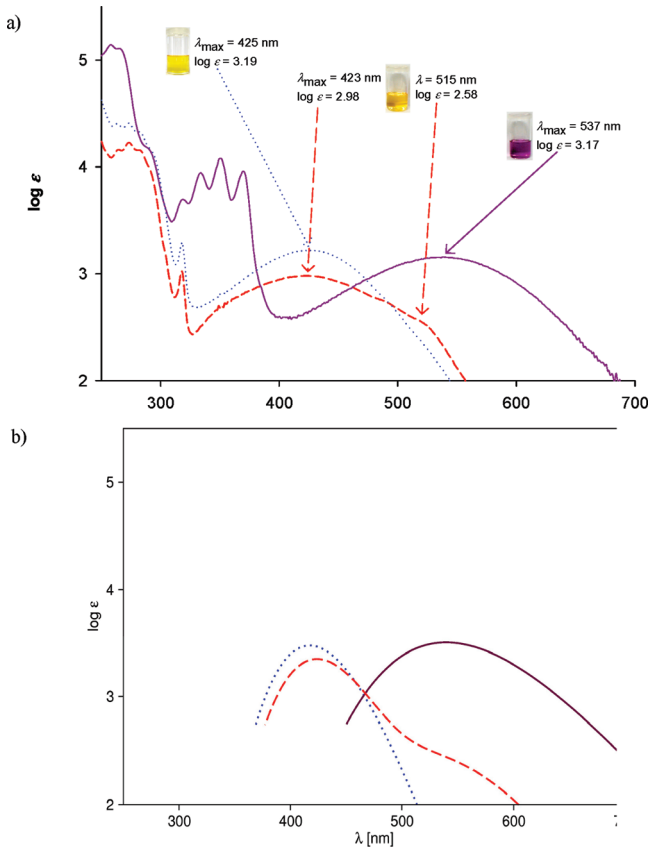

Figure 8. UV/vis spectra of the quinones **1** (solid line), **2** (dashed line), and **3** (dotted line): (a) experimental in $CDCl_3$ at 25 °C, (b) simulated (see text).

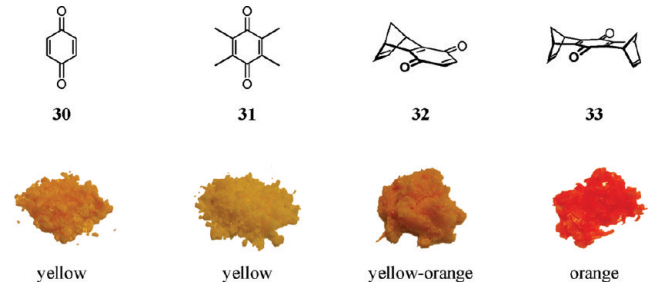

Figure 9. Colors of the solids of the quinones **30**−**33**.

expanded in a correlation-consistent Gaussian basis set of triple-ζ valence quality (cc-pVTZ).[20] For the CC2 calculations, the resolution-of-the-identity (RI) approximation was employed (further computational details are found in the Supporting Information).[21]

Transition energies and corresponding oscillator strengths obtained from the "mixed" velocity-gradient length-velocity formula for *p*-benzoquinone (**30**) are presented in Table 1. Graphical representations of the HF MOs involved in the electronic transitions of **30** may be found in Figure 16. All low energy transitions for **30** shown in Table 1 correspond to transitions into the low-lying π^* LUMO. The first two excited states result from symmetry-forbidden $n \rightarrow \pi^*$ transitions

(19) Christiansen, O.; Koch, H.; Jørgensen, P. *Chem. Phys. Lett.* **1995**, *243*, 409–418.
(20) Dunning, T. H., Jr. *J. Chem. Phys.* **1989**, *90*, 1007–1023.
(21) (a) Hättig, C.; Weigend, F. *J. Chem. Phys.* **2000**, *113*, 5154–5161. (b) Hättig, C.; Köhn, A. *J. Chem. Phys.* **2002**, *117*, 6939–6951.

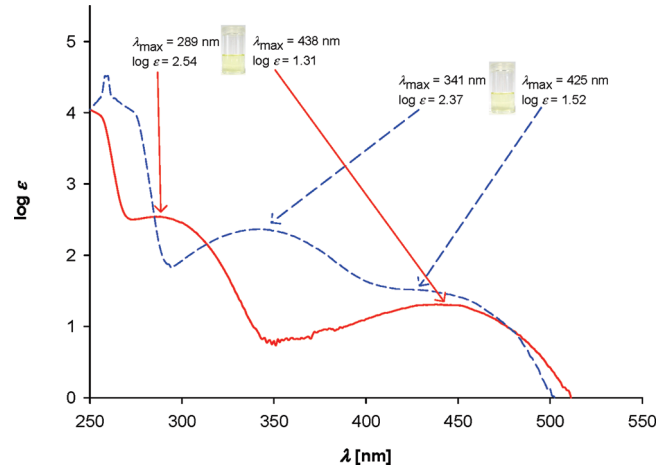

Figure 10. UV/vis spectra of the *p*-benzoquinone **30** (solid line) and duroquinone **31** (dashed line) in $CDCl_3$ at 25 °C.

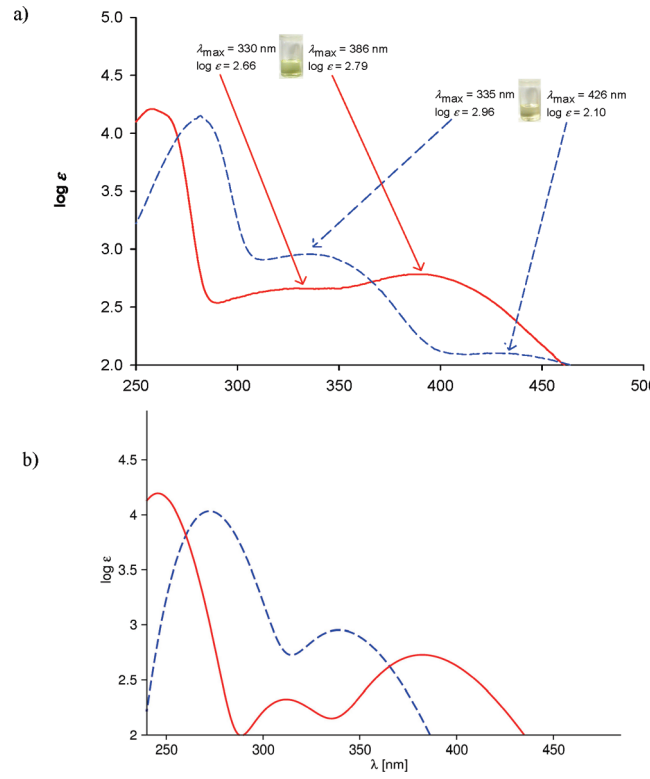

Figure 11. UV/vis spectra of the quinones **32** (solid line) and **33** (dashed line): (a) experimental in $CDCl_3$ at 25 °C, (b) simulated (see text).

starting in antisymmetric and symmetric linear combinations of the lone-pair oxygen orbitals, respectively. Note that the σ orbitals of the carbon backbone also contribute to the *n* orbitals and that they are not the highest occupied HF MOs. The third and fourth excited states result from $\pi \rightarrow \pi^*$ transitions starting from the HOMO and HOMO-1, respectively. Only the fourth transition is symmetry-allowed and displays a large oscillator strength. The complete active space second-order perturbation theory (CASPT2) calculations of Weber et al.[22] yield this state as the seventh excited state. According to CASPT2, the singlet-excited states number four to six are essentially characterized by double excitations. Thus, they cannot be correctly described

(22) Weber, J.; Malsch, K.; Hohlneicher, G. *Chem. Phys. Lett.* **2001**, *264*, 275–318.

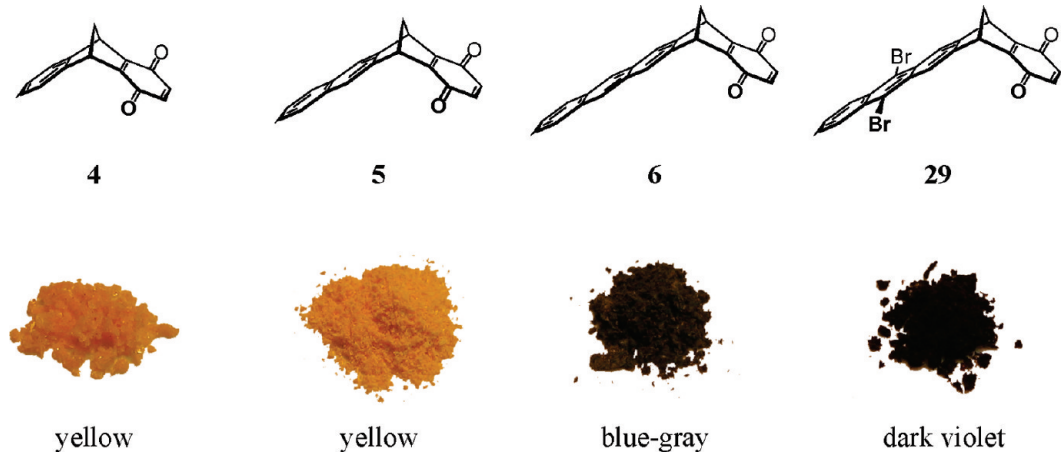

Figure 12. Colors of the solid quinones **4**, **5**, **6**, and **29**. **5** shows a reversible thermochromic color change from yellow to red at 205 °C.

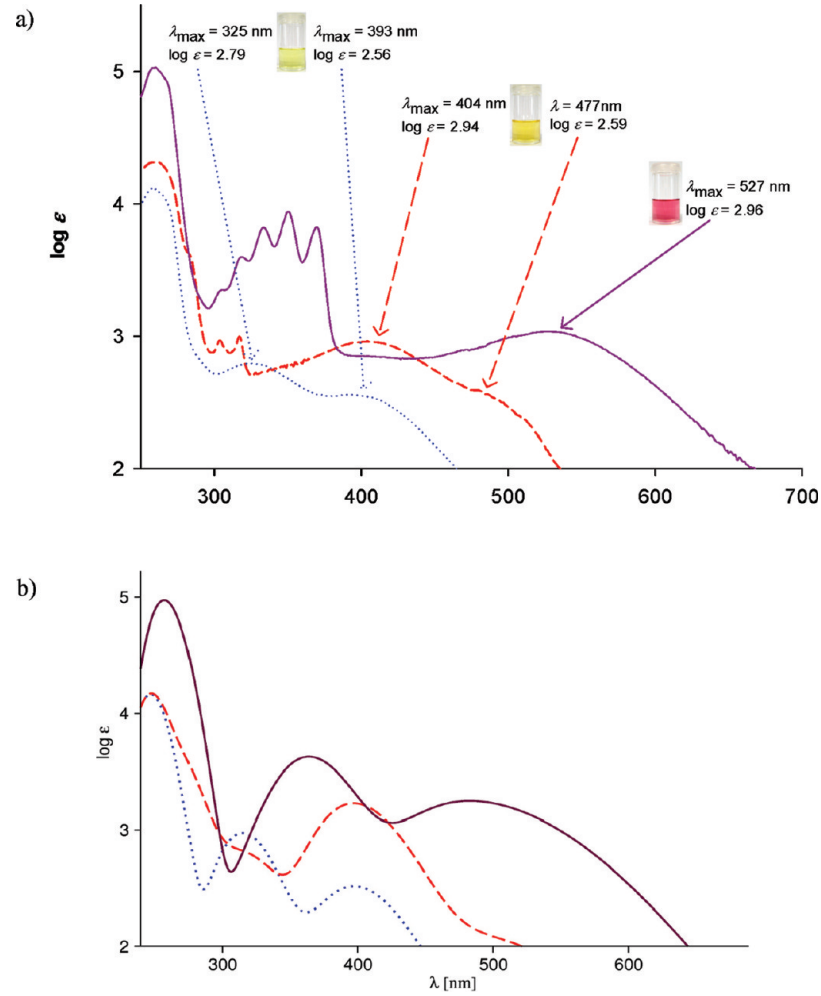

Figure 13. UV/vis spectra of the quinones **4** (dotted line), **5** (dashed line), and **6** (solid line): (a) experimental in $CDCl_3$ at 25 °C, and (b) simulated (see text).

by CC2. Two of the corresponding transitions are symmetry-forbidden; the remaining one was found to have a small oscillator strength of 0.00041. The value of the so-called D1 diagnostics indicating multireference character of the ground state of **30** is found to be 0.08 and thus considerably larger than the largest value of 0.05 recommended for "safe" application of CC2. Comparison with the experimental results given in Table 1 reveals that the calculated excitation energies are overestimated by up to 0.3 eV, which we deem an acceptable error for the series of molecules considered here. The D1 diagnostics for the free arene molecules are below 0.04 and the largest D1 diagnostics of 0.09 for all investigated molecules was found for the *syn*- and *anti*-anthracene clips **1** and **40,** respectively.

In norbornadienoquinone **32**, the symmetry is lowered from D_{2h} to C_s. Thus, all electronic transitions become symmetry-

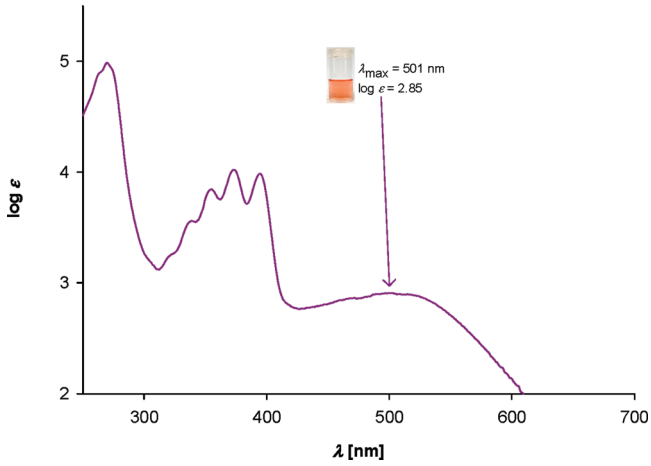

Figure 14. UV/vis spectra of the quinone **29** in $CDCl_3$ at 25 °C.

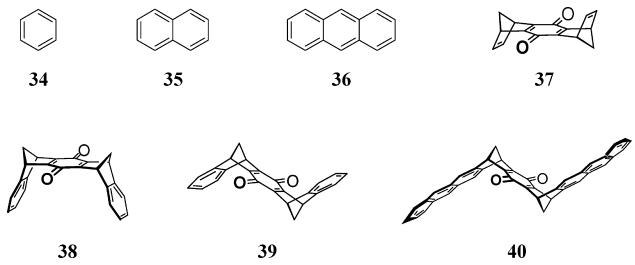

Figure 15. Additional structures of benzene **34**, naphthalene **35**, anthracene **36**, and the quinones **37**−**40** used for quantum chemical calculations.

Table 1. Calculated (CC2/cc-pVTZ) Excited States for *p*-Benzoquinone **30** (cf. Figure 16)[a]

state	$E_{(exp)}$	$E_{(calc)}$	λ	oscil. str.	composition
$1\ ^1B_{2g}$	2.7	2.810	441	-	0.956 ($4b_{1g} \rightarrow 2b_{3g}$)
$1\ ^1A_u$	2.7	2.946	421	-	0.972 ($5b_{3u} \rightarrow 2b_{3g}$)
$1\ ^1B_{1g}$	4.4−4.6	4.645	267	-	0.989 ($1b_{2g} \rightarrow 2b_{3g}$)
$1\ ^1B_{2u}$	5.1−5.4	5.603	221	0.41821	0.961 ($2b_{1u} \rightarrow 2b_{3g}$)

[a] Excitation energies in eV, corresponding wavelengths in nanometers. Only contributions with a coefficient larger than 0.03 are shown.

allowed. The data collected in Table 2 demonstrate, however, that the first two transitions corresponding to $n \rightarrow \pi^*$ transitions within the quinone moiety have low oscillator strengths. They display a bathochromic shift of 10 nm with respect to *p*-benzoquinone **30**. Note that the orbitals 24a′, 18a″, and 19a″ involved in the transition are essentially unaltered *n* and π^* orbitals of *p*-benzoquinone, respectively, as can be seen from Figure 17. This is not true for the occupied orbitals involved in the remaining three transitions: the orbital 25a′ is a linear combination of the two occupied π orbitals of the quinone moiety, denoted as π^+ in the following. The orbitals 26a′ and 27a′ mainly stem from through-space interactions between π orbitals: they are formed by the remaining linear combination π^- of the quinone π orbitals and the π orbital of the norbornadiene rest. Note that orbital 26a′ looks very similar to the orbital denoted as $10a_1$ in norbornadiene, and 27a′ resembles $6b_2$ of norbonadiene, that is, orbitals which to some extent are influenced by π,σ hyperconjugations.[6] The third and fourth transitions (27a′ → 19a″ and 26a′ → 19a″) may be considered as mixtures between a quinone $\pi \rightarrow \pi^*$ excitation and a charge transfer (CT) excitation from an ethene moiety fused to *p*-benzoquinone. These excitations are responsible for the experimentally observed bands with maxima at 386 and 330

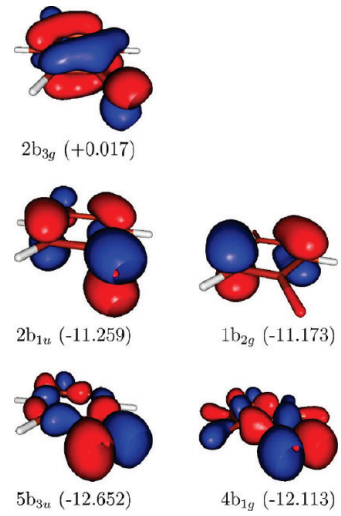

Figure 16. Selected molecular (HF/cc-pVTZ) orbitals of *p*-benzoquinone **30**. Orbital energies in electronvolts (eV).

Table 2. Calculated (CC2/cc-pVTZ) Excited States for **32** (cf. Figure 17)

state	$E_{(calc)}$	λ	oscil. str.	composition
$1\ ^1A'$	2.751	451	0.00010	0.944 (18a″ → 19a″)
$1\ ^1A''$	2.875	431	0.00006	0.966 (24a′ → 19a″)
$2\ ^1A''$	3.493	355	0.00991	0.954 (27a′ → 19a″)
$3\ ^1A''$	4.229	293	0.00389	0.937 (26a′ → 19a″)
$4\ ^1A''$	5.297	234	0.28955	0.929 (25a′ → 19a″)

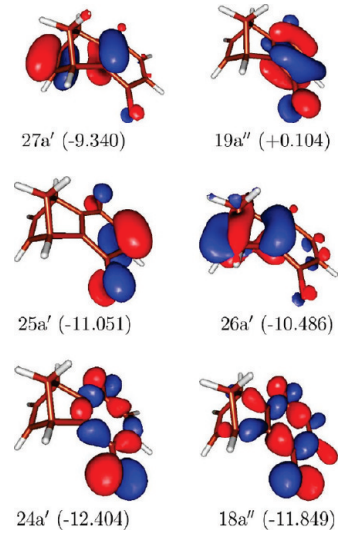

Figure 17. Selected molecular (HF/cc-pVTZ) orbitals of **32**. Orbital energies in electronvolts (eV).

nm, respectively (cf. Figure 11). The remaining fifth transition may be considered as a symmetry-perturbed $\pi \rightarrow \pi^*$ excitation within the quinone moiety. It displays a hypochromic and bathochromic shift of 13 nm with respect to the allowed $\pi \rightarrow \pi^*$ excitation of **30**. Figure 11b shows a simulation of the UV/vis spectra of **30** and **32** based on the results of Tables 1 and 2. All transition energies were down-shifted by 0.25 eV and inhomogeneous broadening of each of the lines was represented through a Gaussian distribution with a width of 0.5 eV (fwhm). The reasonable agreement of the band maxima and of the general shape of the spectrum with experiment (Figure 11a) confirms our calculations and the resulting assignment.

Table 3. Calculated (CC2/cc-pVTZ) Excited States for **4** (cf. Figure 18)

state	$E_{(calc)}$	λ	oscil. str.	composition
1 ^{1}A′	2.734	454	0.00032	0.932 (23a″ → 25a″)
1 ^{1}A″	2.875	431	0.00006	0.964 (31a′ → 25a″)
2 ^{1}A″	3.367	368	0.00607	0.918 (34a′ → 25a″) +0.318 (33a′ → 25a″)
3 ^{1}A″	4.077	304	0.00737	0.895 (33a′ → 25a″) −0.300 (34a′ → 25a″)
2 ^{1}A′	4.248	292	0.01152	0.943 (24a″ → 25a″)
3 ^{1}A′	5.106	243	0.01150	0.716 (34a′ → 35a′) −0.524 (24a″ → 26a″)
4 ^{1}A″	5.269	235	0.26311	0.927 (32a′ → 25a″)

Table 4. Calculated (CC2/cc-pVTZ) Excited States for **5** (cf. Figure S1)

state	$E_{(calc)}$	λ	oscil. str.	composition
1 ^{1}A′	2.710	458	0.00189	0.897 (28a″ → 31a″)
1 ^{1}A″	2.878	431	0.00007	0.955 (37a′ → 31a″)
2 ^{1}A′	3.368	368	0.02539	0.921 (30a″ → 31a″)
2 ^{1}A″	3.389	366	0.00606	0.875 (41a′ → 31a″) +0.420 (40a′ → 31a″)
3 ^{1}A″	4.052	306	0.00731	0.842 (40a′ → 31a″) −0.380 (41a′ → 31a″)
3 ^{1}A′	4.334	286	0.00722	0.703 (41a′ → 42a′) −0.610 (30a″ → 32a″)
4 ^{1}A″	4.823	257	0.05621	0.958 (30a″ → 42a′)
5 ^{1}A″	5.263	236	0.27007	0.925 (39a′ → 31a″)

Table 5. Calculated (CC2/cc-pVTZ) Excited States for **6** (cf. Figure S2)

state	$E_{(calc)}$	λ	oscil. str.	composition
1 ^{1}A′	2.627	472	0.01734	0.695 (33a″ → 37a″) −0.625 (36a″ → 37a″)
1 ^{1}A″	2.878	431	0.00007	0.962 (44a′ → 37a″)
2 ^{1}A′	2.917	425	0.02362	0.718 (36a″ →37a″) +0.625 (33a″ → 37a″)
2 ^{1}A″	3.415	363	0.00702	0.829 (48a′ → 37a″) +0.510 (47a′ → 37a″)
3 ^{1}A″	3.647	340	0.06732	0.980 (36a″ → 49a′)
3 ^{1}A′	3.797	327	0.00798	0.704 (48a′ → 49a′) −0.635 (36a″ → 38a″)
4 ^{1}A″	4.047	306	0.00915	0.752 (47a′ → 37a″) −0.436 (48a′ → 37a″) +0.309 (46a′ → 37a″) −0.309 (45a′ → 37a″)
4 ^{1}A′	4.660	266	0.00001	0.901 (35a′ → 37a″)
5 ^{1}A″	5.058	245	0.00078	0.756 (36a″ → 50a′) +0.611 (35a″ → 49a′)
5 ^{1}A′	5.067	245	1.74606	0.714 (36a″ → 38a″) +0.600 (48a′ → 49a′)

Figure 13b shows a simulation of the UV/vis spectra of the quinones **4**−**6**, the "half-clips", generated in an identical manner using the calculated transition energies and oscillator strengths of Tables 3−5 (for graphical representations of the orbitals, see Figure 18 and Figures S1 and S2 in the Supporting Information). Clearly, the calculations correctly reproduce the observed strong batho- and hyperchromic shift of the first absorption maximum with increasing size of the arene moiety. Much of what has been discussed above also applies to the half-clips. For example, the first, the second, and the seventh excitation in **4** correspond to slightly perturbed $n \rightarrow \pi^*$ and $\pi^+ \rightarrow \pi^*$ excitations within the quinone moiety. Their transition energies are nearly identical to those of the corresponding excitations in **32**. The same holds true for the first, the second, and the eighth transition in **5**, and also for the second excitation in **6**. Note that the small oscillator strength of this second $n \rightarrow \pi^*$ excitation is practically constant along the entire series of molecule **32** and **4**−**6**. The much larger oscillator strength of the $\pi^+ \rightarrow \pi^*$ excitation within the quinone moiety also hardly changes for **32**, **4**, and **5**. However, it is smaller than the oscillator strength of the corresponding transition in **30**, which is easily explained by the fact that the π^+ orbital, loosely speaking, represents only half of that of the π orbitals of **30** from which excitation into π^* is allowed.

As in **32**, the third and fourth electronic states in **4** are found to be mixtures between CT and quinone moiety $\pi \rightarrow \pi^*$ excitations (cf. Table 3). Compared to **32**, the occupied orbitals 33a′ and 34a′ participating in these transitions show a somewhat smaller degree of mixing (cf. Figure 18). The through-space $\pi-\pi$ interactions between the quinone and the benzene moieties now rather become visible at the level of configuration interaction. Note that mixing between two occupied orbitals and configuration mixing become equivalent for single excitations into the same virtual orbital, that is, for the case at hand. A state of essentially pure CT character is observed as the fifth state, labeled as 2 ^{1}A′. The initial orbital of the corresponding transition, the HOMO-1, looks like one component of the degenerate HOMO of benzene **34** (cf. Figure S3). For symmetry reasons, it cannot mix with the occupied π orbitals of the quinone moiety. Finally, the sixth excited state of **4** predominantly results from the lowest $\pi \rightarrow \pi^*$ excitation within the benzene moiety with small admixtures of CT character. It shows a bathochromic shift of 9 nm with respect to the calculated symmetry-forbidden transition into the ^{1}L$_b$ state (the α band) in **34** (cf. Table 6).

The transitions observed in **5** may be characterized in a similar manner. The main differences to **4** are that the 2 ^{1}A′ state of predominant CT character is already found as the third excited state (cf. Table 4). It corresponds to the HOMO → LUMO excitation. Note that the HOMO of **5** is practically identical to the HOMO of naphthalene **35** and that, as in **4**, for symmetry reasons it cannot mix with the occupied π orbitals of the quinone

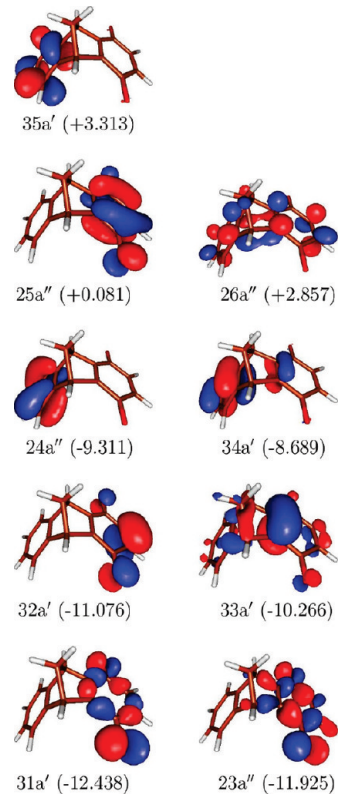

Figure 18. Selected molecular (HF/cc-pVTZ) orbitals of **4**. Orbital energies in electronvolts (eV).

Table 6. Calculated (CC2/cc-pVTZ) Excited States for Benzene **34** (cf. Figure S3)[a]

state	$E_{(exp)}$	$E_{(calc)}$	λ	oscil. str.	composition
1 ^{1}B$_{3u}$ (^{1}L$_b$)	5.06	5.303	234	-	0.700 (1b$_{3g}$ → 1a$_u$) −0.700 (1b$_{2g}$ → 2b$_{1u}$)
1 ^{1}B$_{2u}$ (^{1}L$_a$)	6.44	6.609	188	-	0.699 (1b$_{3g}$ → 2b$_{1u}$) +0.699 (1b$_{2g}$ → 1a$_u$)

[a] Point group D_{2h} (rather than D_{6h}) was used for technical reasons.

Table 7. Calculated (CC2/cc-pVTZ) Excited States for Naphthalene **35** (cf. Figure S4)

state	$E_{(exp)}$	$E_{(calc)}$	λ	oscil. str.	composition
1 $^1B_{3u}$ (^1L_b)	4.13	4.438	279	0.00003	0.699 ($2b1_u \rightarrow 2b_{2g}$) −0.699 ($1a_u \rightarrow 2b_{3g}$)
1 $^1B_{2u}$ (^1L_a)	4.66	4.834	256	0.08117	0.968 ($1a_u \rightarrow 2b_{2g}$)

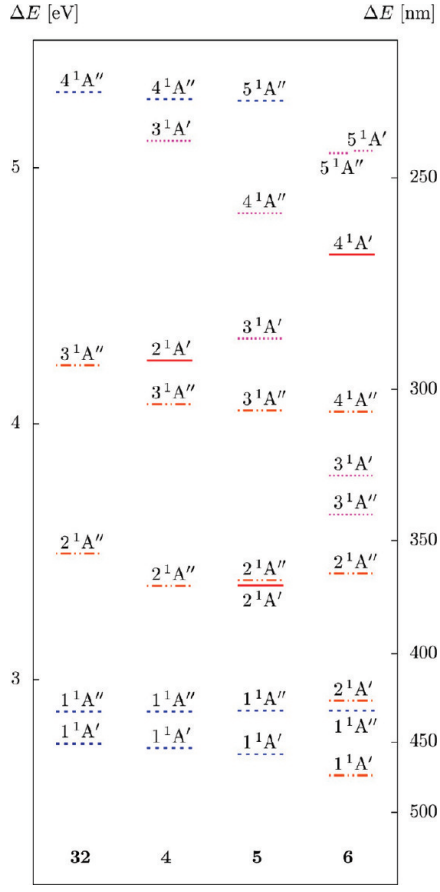

Figure 19. Calculated levels of the half-clip quinones. Solid lines denote states of predominant CT character, dashed lines quinone moiety excitations, dashed-dotted lines states with partial CT character, and dotted lines arene moiety excitations.

moiety (cf. Figures S1 and S4). Furthermore, there are two states of essentially pure naphthalene moiety $\pi \rightarrow \pi^*$ character with energies below that of the intense quinone moiety $\pi \rightarrow \pi^*$ transition. While the lower one (3 $^1A'$) of these shows a bathochromic shift of 7 nm with respect to excitation into the ^1L_b state in **35**, the wavelength of the second one (4 $^1A''$) is practically the same as that of excitation into the ^1L_a state giving rise to the *p* band (cf. Table 7).

The findings for norbornadienoquinone **32**, and its benzo- or naphtho-substituted derivatives **4** and **5**, respectively, discussed above are collected in Figure 19. As can be seen from the figure, there is a slight lowering of the energy of the first excited state (1 $^1A'$) along this series. A slight, yet increasing amount of mixing with CT excitations is responsible for this effect. This becomes obvious for the lowest transition in the anthraceno-substituted system **6** which displays a marked bathochromic shift of 31 nm with respect to parent *p*-benzoquinone **30** and, in particular, a strong increase of its oscillatory strength (cf. Table 5). Here, the CT excitation out of the HOMO, which looks like the HOMO of anthracene **36** (cf. Figures S2 and S5), mixes with the first $n \rightarrow \pi^*$ excitation of the quinone moiety. The

Table 8. Calculated (CC2/cc-pVTZ) Excited States for **36** (cf. Figure S5)

state	$E_{(exp)}$	$E_{(calc)}$	λ	oscil. str.	composition
1 $^1B_{2u}$ (^1L_a)	3.60	3.625	342	0.07740	0.982 ($2b_{3g} \rightarrow 3b_{1u}$)
1 $^1B_{3u}$ (^1L_b)	3.64	3.865	321	0.00034	0.703 ($2b_{2g} \rightarrow 3b_{1u}$) −0.690 ($2b_{3g} \rightarrow 2a_u$)
1 $^1B_{1g}$		5.108	243	-	0.831 ($1a_u \rightarrow 3b_{1u}$) +0.525 ($2b_{3g} \rightarrow 3b_{2g}$)
2 $^1B_{1g}$		5.304	234	-	0.828 ($2b_{3g} \rightarrow 3b_{2g}$) −0.522 ($1a_u \rightarrow 3b_{1u}$)
2 $^1B_{3u}$		5.417	229	2.25389	0.703 ($2b_{3g} \rightarrow 2a_u$) +0.684 ($2b_{2g} \rightarrow 3b_{1u}$)

Table 9. Calculated (CC2/cc-pVTZ) Excited States for **33** (cf. Figure 20)

state	$E_{(calc)}$	λ	oscil. str.	composition
1 $^1B_1$	2.696	460	0.00048	0.933 ($10a_2 \rightarrow 15b_2$)
1 $^1A_2$	2.799	443	-	0.938 ($15b_1 \rightarrow 15b_2$)
2 $^1A_2$	2.991	415	-	0.957 ($17b_1 \rightarrow 15b_2$)
1 $^1B_2$	3.904	318	0.01664	0.950 ($21a_1 \rightarrow 15b_2$)
3 $^1A_2$	3.977	312	-	0.941 ($16b_1 \rightarrow 15b_2$)
2 $^1B_2$	4.802	258	0.20048	0.906 ($20a_1 \rightarrow 15b_2$)

second $n \rightarrow \pi^*$ excitation, on the other hand, is still found at the same transition energy as in the other half-clips. It is slightly lower than the excitation energy of the remaining linear combination 2 $^1A'$ of quinone moiety $n \rightarrow \pi^*$ and CT excitations. The transition into 2 $^1A'$ also has a noticeable oscillator strength and is the main contributor to the low-energy band in the spectrum of **6** (cf. Figure 13). Figure 19 demonstrates that the next state, 2 $^1A''$, has a fairly constant energy for all of the half-clips. As mentioned above, this state is a linear combination of a CT and a quinone moiety $\pi \rightarrow \pi^*$ excitation. The other linearly independent combination of these two excitations gives rise to the 3 $^1A''$ state in **32**, **4**, and **5**, while the corresponding state in **6** is dubbed 4 $^1A''$. Again, its energy is fairly constant for all of the half-clips. In **6**, the 2 $^1A''$ and 4 $^1A''$ states are separated by two states which predominantly stem from $\pi \rightarrow \pi^*$ excitations within the anthracene moiety. The corresponding excitations in anthracene **36** give rise to the nearly degenerate ^1L_a and ^1L_b states, respectively (cf. Table 8). With respect to these, one observes only a slight bathochromic shift of a few nanometers in **6**. There is one essentially "pure" CT state (4 $^1A'$) in **6**, at a fairly high energy of 4.66 eV. We stopped our calculations at the first state (5 $^1A'$) with an oscillator strength larger than 0.2. It is of predominant $\pi \rightarrow \pi^*$ anthracene character, like its nearly degenerate companion 5 $^1A''$. Note that the latter is the only state in any of the half-clips which shows a down-shift of more than 0.1 eV when diffuse basis functions are added (cf. Table S1), indicating that Rydberg mixing plays a role here (as it also does for the higher excited states of **36** not given in Table S1).

For the quinone **33** and the clips **38**, **2**, and **1**, only the first few transitions were considered, as for the corresponding anti-configured isomers **37**, **39**, **3**, and **40** which, for convenience, will be dubbed "anti-clips" in the following. Concentrating first on **33** and **37**, Tables 9 and 10 and Figures 20 and 21, respectively, demonstrate that the first two transitions in each case correspond to $n \rightarrow \pi^*$ excitations within the quinone moiety. All of the remaining transitions should best be qualified as mixtures between $\pi \rightarrow \pi^*$ excitations within the quinone moiety and CT excitations from appropriate symmetric and antisymmetric linear combinations of the π orbitals on the norbonadiene rests.

Table 10. Calculated (CC2/cc-pVTZ) Excited States for **37** (cf. Figure 21)

state	$E_{(calc)}$	λ	oscil. str.	composition
$1\ ^1A_g$	2.695	460	-	0.933 ($11b_g \rightarrow 12b_g$)
$1\ ^1A_u$	2.810	441	0.00015	0.959 ($16b_u \rightarrow 12b_g$)
$1\ ^1B_g$	2.999	413	-	0.970 ($20a_g \rightarrow 12b_g$)
$2\ ^1A_u$	3.737	332	0.00690	0.933 ($18b_u \rightarrow 12b_g$)
$2\ ^1B_g$	4.235	293	-	0.950 ($19a_g \rightarrow 12b_g$)
$3\ ^1A_u$	4.712	263	0.20699	0.902 ($17b_u \rightarrow 12b_g$)

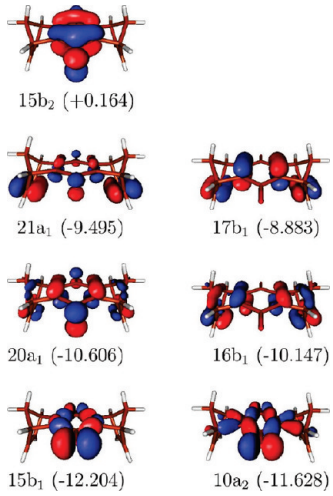

Figure 20. Selected molecular (HF/cc-pVTZ) orbitals of **33**. Orbital energies in electronvolts (eV).

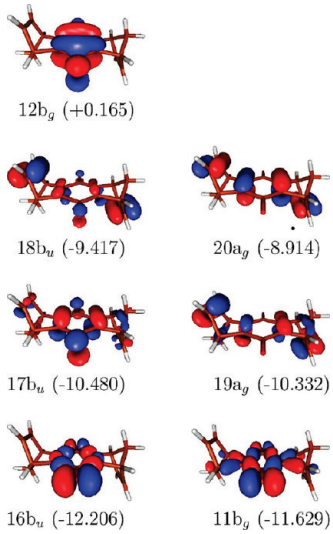

Figure 21. Selected molecular (HF/cc-pVTZ) orbitals of **37**. Orbital energies in electronvolts (eV).

The mixing here becomes visible in the mixing of the orbitals, with a direct participation of quinone π orbitals (rather than of π^+ and π^- orbitals as for the half-clips). For both **33** and **37**, inspection of the orbitals suggests that for the fourth state the CT character somewhat prevails while it is the quinone moiety $\pi \rightarrow \pi^*$ character for the sixth state. The most important difference between **33** and **37** is found for the oscillator strengths: in the C_{2v} point group of **33**, all transitions become symmetry-allowed, except for transitions into states of A_2 symmetry, while for **37** with its C_{2h} point group, only transitions into states of A_u and B_u symmetry are allowed. In consequence, while for **33** the first electronic transition is allowed and the second is symmetry-forbidden, in **37**, it is the other way round. This should lead to a hypsochromic shift of about 20 nm for the first band between **33** and **37**, despite the virtually identical energies of the first two electronically excited states. Note, however, that vibronic coupling, which could not be taken into account in this study, will influence the transition intensities. This may explain the seeming absence of the experimentally observed low-energy maximum at 426 nm in the simulated spectrum of **33** shown in Figure 11b: without vibronic coupling, the oscillator strength of the first transition is calculated too low.

Table 11. Calculated (CC2/cc-pVTZ) Excited States for **38** (cf. Figure S6)

state	$E_{(calc)}$	λ	oscil. str.	composition
$1\ ^1B_1$	2.655	467	0.00111	0.906 ($15a_2 \rightarrow 21b_2$)
$1\ ^1A_2$	2.789	445	-	0.901 ($22b_1 \rightarrow 21b_2$)
$2\ ^1A_2$	2.915	425	-	0.877 ($24b_1 \rightarrow 21b_2$) +0.347 (23b1 $\rightarrow 21b_2$)
$1\ ^1B_2$	3.545	350	0.00609	0.976 ($28a_1 \rightarrow 21b_2$)
$3\ ^1A_2$	3.786	327	-	0.881 ($23b_1 \rightarrow 21b_2$) −0.368 (24b1 $\rightarrow 21b_2$)
$2\ ^1B_1$	4.113	301	0.00644	0.936 ($16a_2 \rightarrow 21b_2$)
$1\ ^1A_1$	4.123	301	0.01404	0.972 ($20b_2 \rightarrow 21b_2$)

Table 12. Calculated (CC2/cc-pVTZ) Excited States for **39** (cf. Figure S7)

state	$E_{(calc)}$	λ	oscil. str.	composition
$1\ ^1A_g$	2.659	466	-	0.908 ($16b_g \rightarrow 18b_g$)
$1\ ^1A_u$	2.809	441	0.00013	0.954 ($23b_u \rightarrow 18b_g$)
$1\ ^1B_g$	2.935	423	-	0.893 ($27a_g \rightarrow 18b_g$) +0.427 ($26a_g \rightarrow 18b_g$)
$2\ ^1A_u$	3.484	356	0.00381	0.964 ($25b_u \rightarrow 18b_g$)
$2\ ^1B_g$	3.955	313	-	0.883 ($26a_g \rightarrow 18b_g$) −0.397 ($27a_g \rightarrow 18b_g$)
$2\ ^1A_g$	4.154	298	-	0.937 ($17b_g \rightarrow 18b_g$)
$1\ ^1B_u$	4.169	297	0.02261	0.971 ($19a_u \rightarrow 18b_g$)

Table 13. Calculated (CC2/cc-pVTZ) Excited States for **2** (cf. Figure S8)

state	$E_{(calc)}$	λ	oscil. str.	composition
$1\ ^1B_1$	2.590	479	0.00466	0.819 ($20a_2 \rightarrow 27b_2$) +0.428 ($22a_2 \rightarrow 27b_2$)
$1\ ^1A_2$	2.790	444	-	0.882 ($28b_1 \rightarrow 27b_2$)
$2\ ^1A_2$	2.929	423	-	0.823 ($31b_1 \rightarrow 27b_2$) +0.455 ($30b_1 \rightarrow 27b_2$)
$1\ ^1A_1$	3.157	393	0.02867	0.974 ($26b_2 \rightarrow 27b_2$)
$2\ ^1B_1$	3.222	385	0.01281	0.871 ($22a_2 \rightarrow 27b_2$) −0.417 ($20a_2 \rightarrow 27b_2$)

Table 14. Calculated (CC2/cc-pVTZ) Excited States for **3** (cf. Figure S9)

state	$E_{(calc)}$	λ	oscil. str.	composition
$1\ ^1A_g$	2.608	475	-	0.838 ($21b_g \rightarrow 24b_g$) +0.387 ($23b_g \rightarrow 24b_g$)
$1\ ^1A_u$	2.812	441	0.00013	0.933 ($29b_u \rightarrow 24b_g$)
$1\ ^1B_g$	2.954	420	-	0.825 ($34a_g \rightarrow 24b_g$) +0.548 ($33a_g \rightarrow 24b_g$)
$1\ ^1B_u$	3.221	385	0.05487	0.972 ($25a_u \rightarrow 24b_g$)
$2\ ^1A_g$	3.274	379	-	0.889 ($23b_g \rightarrow 24b_g$) −0.377 ($21b_g \rightarrow 24b_g$)

The results for the clips **38**, **2**, and **1** and the anti-clips **39**, **3**, and **40** are collected in Tables 10−16, and corresponding level schemes including a qualitative characterization of the states are presented in Figures 22 and 23, respectively.

Table 15. Calculated (CC2/cc-pVTZ) Excited States for **1** (cf. Figure S10)

state	$E_{(calc)}$	λ	oscil. str.	composition
1 $^1B_1$	2.400	517	0.01784	0.790 ($28a_2 \rightarrow 33b_2$) +0.507 ($25a_2 \rightarrow 33b_2$)
1 $^1A_1$	2.581	480	0.04296	0.971 ($32b_2 \rightarrow 33b_2$)
1 $^1A_2$	2.791	444	-	0.897 ($35b_1 \rightarrow 33b_2$)
2 $^1B_1$	2.833	438	0.00551	0.753 ($25a_2 \rightarrow 33b_2$) −0.553 ($28a_2 \rightarrow 33b_2$)
2 $^1A_2$	2.941	422	-	0.775 ($38b_1 \rightarrow 33b_2$) +0.537 ($37b_1 \rightarrow 33b_2$)

Table 16. Calculated (CC2/cc-pVTZ) Excited States for **40** (cf. Figure S11)

state	$E_{(calc)}$	λ	oscil. str.	composition
1 ^1A_g	2.466	503	-	0.728 ($29b_g \rightarrow 30b_g$) +0.579 ($26b_g \rightarrow 30b_g$)
1 ^1B_u	2.663	466	0.08481	0.969 ($31a_u \rightarrow 30b_g$)
1 ^1A_u	2.815	440	0.00013	0.952 ($36b_u \rightarrow 30b_g$)
2 ^1A_g	2.862	433	-	0.700 ($26b_g \rightarrow 30b_g$) −0.628 ($29b_g \rightarrow 30b_g$)
1 ^1B_g	2.976	417	-	0.763 ($41a_g \rightarrow 30b_g$) +0.633 ($40a_g \rightarrow 30b_g$)

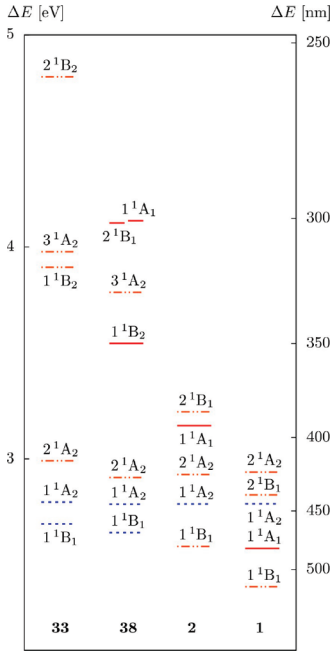

Figure 22. Calculated levels of the clip quinones. Solid lines denote states of predominant CT character, dashed lines quinone moiety excitations, and dashed-dotted lines states with partial CT character.

The main differences of the clips and anti-clips with respect to the half-clips are the higher symmetry and the larger number of arene moiety π orbitals participating in the electronic transitions. These form symmetric and antisymmetric linear combinations, respectively, which in turn may mix with the two quinone π orbitals. In **38** and in **39**, respectively, this leads to a low-lying state of mixed CT and quinone moiety $\pi \rightarrow \pi^*$ character as the third excited state. Corresponding 2 $^1A_2$ and 1 ^1B_g states, respectively, are also found for the remaining clips and anti-clips. Transitions into these states are symmetry-forbidden. The first two excited states in **38** and **39**, respectively, essentially are only slightly perturbed quinone moiety $n \rightarrow \pi^*$ transitions. For the lowest state of **1**, **2**, **3**,, and **40**, however, mixing in of CT character becomes evident at the configuration

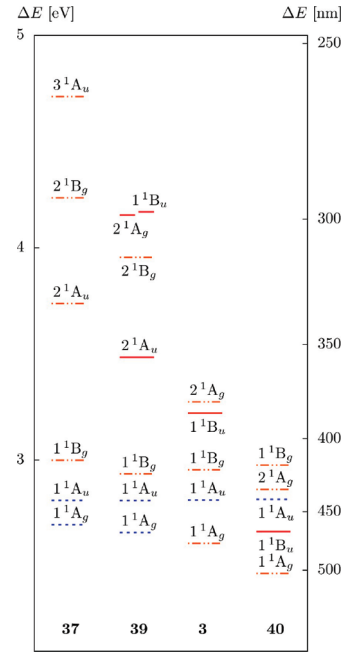

Figure 23. Calculated levels of the clip quinones. Solid lines denote states of predominant CT character, dashed lines quinone moiety excitations, and dashed-dotted lines states with partial CT character.

interaction level (cf. Tables 12−15). The other state of quinone moiety $n \rightarrow \pi^*$ character does not suffer from mixing at the orbital or configuration interaction level. It thus has a virtually constant transition energy for all of the clips and anti-clips. In **1** and **40**, this leads to the situation that it becomes the third excited state, after a state of predominant CT character as the second excited state. As already discussed above for **38** and **39**, electronic transitions into the lowest excited state are symmetry-allowed for the clips, while they are forbidden for the anti-clips. This explains the "shoulder" at 515 nm in the experimental spectrum of **2**, which is absent in the spectrum of the corresponding anti-configured isomer **3** (cf. Figure 8), as can be seen from the comparison with the simulated low-energy part of the spectra shown in Figure 8b (based on the data in Tables 12−14, employing a down-shift of 0.25 eV and Gaussian broadening with width 0.5 eV). Note that most of the intensity of the low-energy band in **1** is due to the transition into the second excited state, that is, the lowest state of essentially pure CT character. The transition into the first excited state is not visible as a separate band but rather helps to broaden the low-energy band.

Conclusion

The novel surprisingly colorful dark blue and orange-red molecular clips **1** and **2** were synthesized by DDQ oxidation of the corresponding colorless hydroquinone clips **7** and **9**. The colors of the quinone clips result from broad absorption bands in the visible range (**1**, $\lambda_{max} = 537$ nm, and **2**, $\lambda_{max} = 423$ and $\lambda_{shoulder} = 515$ nm) showing bathochromic shifts of 112 and 90 nm, respectively, compared to the similarly tetraalkyl-substituted duroquinone **31**, even though the clips **1** and **2** only contain insulated π systems as chromophores, a central tetraalkyl-substituted *p*-benzoquinone spacer-unit, and two anthracene or two naphthalene sidewalls. To elucidate the electronic properties of these clips, we prepared the compound **3**, the anti-configured isomer of clip **2**, and the benzene-, naphthalene-, and anthracene-substituted quinones **4**, **5**, and **6**, the so-called "half-clips". The

"half-clips" **6** and **5** show a similar color change and the same trend in the UV/vis absorption spectra as the anthracene and naphthalene clip **1** and **2**. This finding already rules out that the color of these systems is a result of "through-space" $\pi-\pi$ interactions between the aromatic sidewalls in the molecular clips **1** and **2**. The UV/vis spectra of the molecular clips **1**−**3** (Figure 8), the "half-clips" **4**−**6** (Figure 13), and the quinones **32** and **33** (Figure 11) simulated by means of quantum chemical *ab initio* calculations agree well with the experimental spectra. The quantum chemical calculations allow the following conclusions: The bathochromic shift of the absorption band at the longest wavelength in the "half-clip" quinones **4**, **5**, and **6** with the increasing number of rings in the anellated aromatic unit (from benzene to anthracene) is the result of an increasing configuration interaction between a $n \rightarrow \pi^*$ excitation of the quinoid component and a $\pi \rightarrow \pi^*$ excitation with intramolecular charge transfer (CT) character. The initial π orbitals involved in the various transitions mainly stem from through-space interactions between π orbitals of the aromatic sidewalls and π orbitals of the quinone moiety with varying degree of mixing. The configuration interaction in the excited states can be considered to be a homoconjugation, that is, the relevant charge transfer states are formed across an allegedly insulating aliphatic bridge. The increasing CT character of the absorption band at the longest wavelength in UV/vis spectra of the "half-clip" quinones **4**, **5**, and **6** is consistent with the decreasing redox potential of benzene, naphthalene, and anthracene toward *p*-benzoquinone, which is also reflected by the absorption band in the UV/vis spectra of the intermolecular CT complexes between *p*-benzoquinone and naphthalene ($\lambda_{max} = 373$ nm) or anthracene ($\lambda_{max} = 450$ nm). The bathochromic shift of absorption band at the longest wavelength in the UV/vis spectra of the naphthalene clips **2** and **3** to the anthracene clip **1** can be explained analogously to that observed in the spectra of the corresponding "half-clips" **5** and **6**.

Acknowledgment. We gratefully acknowledge financial support by the Deutsche Forschungsgemeinschaft.

Supporting Information Available: Details on the quantum chemical calculations including plots of relevant molecular orbitals, experimental details, ^{1}H NMR spectra of the new compounds, and supplementary crystallographic data (cif files). This material is available free of charge via the Internet at http://pubs.acs.org.

JA910362J